Section II

Chapter 4: Results and Discussion

4. Results and Discussion

The work carried out in this section is discussed under two main heads:

4.1 Chemical work

4.2 Biological studies

4.1 Chemical Work

The compounds were synthesized as per the general **Scheme 4.1** in which diverse substitutions were used for the synthesis of quinazolinones having guanidine pharmacophore in the ring system.

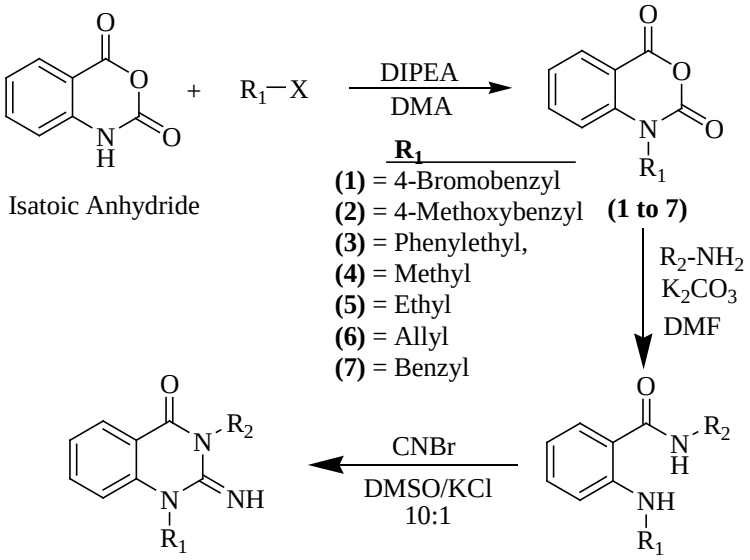

R_1
4-Bromobenzyl
4-Methoxybenzyl
Phenylethyl
Methyl
Ethyl
Allyl
Benzyl

R_2
Phenylethyl,
Isobutyl,
Butyl,
4-Methylbenzyl,
Isopropyl,
Propyl,
Cyclopropyl,
Benzyl,
4-Methoxybenzyl,
2-Chlorobenzyl,
2-Furylmethyl

Scheme 4.1 Synthetic scheme for (1*H*)-2-imino-2,3-dihydroquinazolin-4-ones (**50-91**)

The desired compounds (1*H*)-2-imino-2,3-dihydroquinazolin-4-ones(**50-91**), were synthesized from isatoic anhydride in three steps. In the first step, isatoic anhydride was

reacted with alkyl halides in presence of organic base like DIPEA (*N*,*N*-diisopropylethylamine) to generate *N*-alkyl substituted isatoic anhydrides (**1-7**). The substituted isatoic anhydrides were subjected to ring opening by reaction with primary amines to afford 2-amino benzamide derivatives (**8-49**). The synthesized 2-amino benzamide derivatives were cyclised using cyanogens bromide for the synthesis of (1*H*)-2-imino-2,3-dihydroquinazolin-4-ones.

The detailed description of the work carried out towards achieving the proposed plan has been discussed under the following headings:

4.1.1 Synthesis of different *N*-substituted isatoic anhydrides (**1-7**)

4.1.2 Synthesis of substituted 2-aminobenzamides (**8-49**)

4.1.3 Synthesis of 1,3-disubstituted 2-imino-2,3-dihydro-4-quinazolinones (**50-91**)

4.1.1 Synthesis of different *N*-substituted isatoic anhydrides (1-7)

Isatoic anhydride when reacted with different aryl/alkyl halide in presence of diisopropylethyl amine (DIPEA) and *N*,*N*-dimethyl acetamide (DMA) offered different *N*-substituted isatoic anhydrides (**1-7**). The reaction mechanism involves aliphatic nucleophilic substitution which requires a base DIPEA to enhance the reactivity. DMA as a polar aprotic solvent increases the rate of the SN_2 reaction.

In case of methyl, benzyl, 4-bromobenzyl and allyl substituents, the reaction mixture was stirred at room temp for 2-3 hrs whereas for ethyl, phenylethyl and 4-methoxybenzyl substituents, elevated temp (80-100^{o}C) for 2-3 hrs was required for the completion of the reaction. Progress of the reaction was monitored by TLC using hexane:EtOAc (6:4) as the mobile phase and the crude products were recrystalized from methanol to obtain compounds pure enough for the next reaction.

IR spectra of the compounds confirmed the formation of intermediates (**1-7**) as N-H stretching vibration peak of isatoic anhydride disappeared in *N*-substituted isatoic anhydrides and two stretching vibration peaks for carbonyl groups of the anhydrides were intact in the corresponding substituted isatoic anhydrides. IR spectra show peaks in the range of 1780-1760 cm^{-1} and 1725-1715 cm^{-1} for carbonyl stretching of isatoic anhydrides.

All the synthesized compounds (**1-7**) show peaks in the range of 1300-900 cm^{-1} due to C-O stretching.

4.1.2 Synthesis of substituted 2-aminobenzamides (8-49)

Various substituted 2-aminobenzamides (**8-49**) were synthesized from *N*-substituted isatoic anhydrides in one step by addition of amines. Different amines were used for nucleophilic attack on carbonyl carbon of *N*-substituted isatoic anhydride. Nucleophile preferably attacks on C_4 carbon of ring rather than C_2 carbon of the ring as adjacent N_1 nitrogen enhances the electron density at C_2 carbon whereas oxygen in the ring makes C_4 carbonyl carbon more susceptible to nucleophilic attack. Rate of the reaction can be enhanced by addition of inorganic base like potassium carbonate as it neutralizes the evolved acidic components. A polar aprotic solvent like *N*,*N*-dimethylformamide (DMF) increases the rate of reaction. The reaction mixtures were stirred at 45^{o}C for 45 minutes. The completion of reaction was confirmed by TLC using hexane:EtOAc (7:3) as the mobile phase and the products were recrystallized from methanol:chloroform to obtain 2-aminobenzamides (**8-49**). The yields of the products (**8-49**) and their melting points are listed in Table 4.1.

Table 4.1: Synthesis of various substituted aminobenzamides

Compound	R_1	R_2	Yield (%)	m.p. (^{o}C)
8	4-Bromobenzyl	Phenylethyl	89.3	118-120
9		Isobutyl	89.5	114-117
10		Butyl	89.3	100-104
11		4-Methylbenzyl	88.2	140-142
12		Isopropyl	88.4	125-129
13		Propyl	89.6	103-106
14		Cyclopropyl	88.4	122-124
15		Benzyl	88.6	160-162
16		2-Chlorobenzyl	89.3	137-141
17	4-Methoxybenzyl	Phenylethyl	90.5	99-102
18		Isobutyl	87.3	98-102

19		Butyl	88.2	100-104
20		4-Methylbenzyl	89.5	108-111
21		Isopropyl	88.1	100-107
22		Benzyl	89.7	115-118
23		4-Methoxybenzyl	90.5	110-113
24		2-Chlorobenzyl	88.3	98-102
25		2-Furylmethyl	88.7	105-110
26	Phenylethyl	Phenylethyl	90.3	94-96
27		Isobutyl	88.2	92-94
28		Butyl	89.4	85-87
29		4-Methylbenzyl	88.8	107-110
30		Propyl	88.1	65-68
31		Benzyl	88.3	107-110
32		4-Methoxybenzyl	87.6	88-90
33		2-Chlorobenzyl	91.3	114-118
34	Methyl	Phenylethyl	91.3	177-180
35		Isobutyl	88.5	143-146
36		4-Methylbenzyl	91.3	178-180
37		Propyl	89.3	149-151
38		2-Chlorobenzyl	87.9	>200
39	Ethyl	4-Methylbenzyl	91.5	100-102
40	Allyl	Isobutyl	87.5	145-147
41		Isopropyl	91.1	146-148
42		Cyclopropyl	89.3	164-167
43		Benzyl	88.5	177-179
44		2-Chlorobenzyl	90.3	>200
45	Benzyl	Isobutyl	89.1	160-163
46		4-Methylbenzyl	89.2	112-115
47		Propyl	89.5	108-112
48		Benzyl	86.6	186-188
49		2-Chlorobenzylamine	89.3	>200

IR spectras of these compounds (**8-49**) showed N-H stretching peaks near 3300 cm^{-1}. The carbonyl C=O stretching was observed near 1625 cm^{-1}. Two N-H bending peaks near 1540 and 1515 cm^{-1} along with bands at 820, 750 and 700 cm^{-1} due to *p*-disubstituted, *o*-disubstituted and mono-substituted benzene rings were observed.

4.1.3 Synthesis of 1, 3-disubstituted 2-imino-2,3-dihydro-4-quinazolinones (50-91)

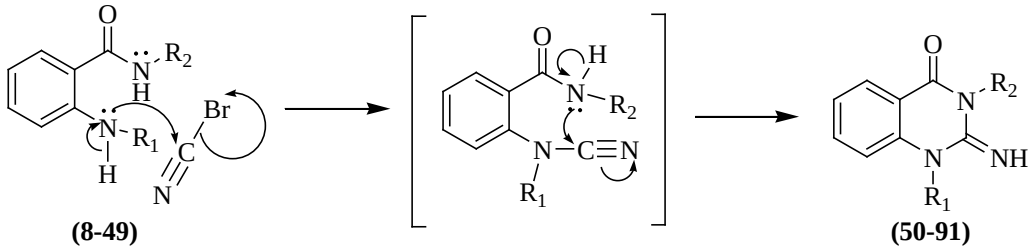

(8-49) **(50-91)**

Scheme 4.2: Synthesis of 1, 3-disubstituted 2-imino-2,3-dihydro-4-quinazolinones

Cyclization of *N*-substituted 2-aminobenzamides with cyanogen bromide resulted in the formation of 1,3-disubstituted 2-imino-2,3-dihydro-4-quinazolinones (**50-91**). The reaction was carried out by stirring *N*-substituted 2-aminobenzamides with cyanogen bromide in DMSO:KCl (10:1) at elevated temp (80-100^{o}C). Amino nitrogen of 2-amino-benzamides first attacked the positively charged carbon atom of cyano electrophile and then further attack by nitrogen of benzamide on the same carbon resulted in the formation of cyclized product. Progress of the reaction was monitored by the TLC. The synthesized quinazolinones were recrystalized from methanol and characterized by spectral techniques.

1-(4-Bromobenzyl)-3-phenethyl-2-imino-2,3-dihydroquinazolin-4(1*H*)-one **(50)** showed IR characteristic peaks at 3296 (N-H str), 1603 (C=O str) and 1553 cm^{-1}(C=N str). Its ^{1}H-NMR spectrum displayed signals at δ 8.46 (s, 1H, NH_{j}), 8.10-7.10 (m, 13H, Ar$H_{a\text{-}i}$), 5.33 (s, 2H, CH_{2k}), 3.82-3.77 (m, 2H, CH_{2l}) and 3.01 (t, 2H, CH_{2m}). Its mass spectrum showed characteristic peaks at m/z 434 (M+) and 436 (M+2).

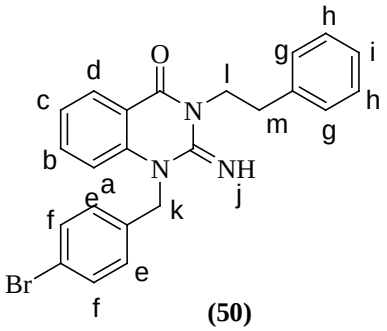

(50)

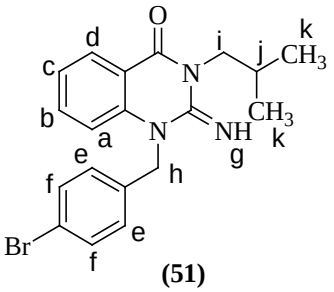

(51)

1-(4-Bromobenzyl)-3-isobutyl-2-imino-2,3-dihydroquinazolin-4(1*H*)-one **(51)** showed IR characteristic peaks at 3287 (N-H str), 1617 (C=O str) and 1537 cm^{-1}(C=N str). Its ^{1}H-NMR spectrum displayed signals at δ 7.55-6.83 (m, 8H, Ar$H_{a\text{-}f}$), 5.84 (s, 1H, NH_g), 5.45 (s, 2H, CH_{2h}), 3.57 (d, 2H, CH_{2i}), 2.07-2.00 (m, 1H, CH_j) and 1.04 (d, 6H, CH_{3k}). Its mass spectrum showed characteristic peaks at m/z 386 (M+) and 388 (M+2).

1-(4-Bromobenzyl)-3-butyl-2-imino-2,3-dihydroquinazolin-4(1*H*)-one **(52)** showed IR characteristic peaks at 3283 (N-H str), 1620 (C=O str) and 1541cm^{-1}(C=N str).

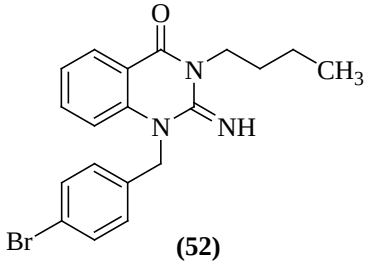

(52)

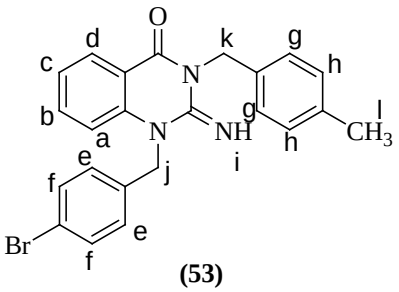

(53)

1-(4-Bromobenzyl)-3-(4-methylbenzyl)-2-imino-2,3-dihydroquinazolin-4(1*H*)-one **(53)** showed IR characteristic peaks at 3257 (N-H str), 1639 (C=O str) and 1536 cm^{-1}(C=N str). Its ^{1}H-NMR spectrum displayed signals at δ 7.56-7.07 (m, 12H, Ar$H_{a\text{-}h}$), 5.37 (s, 1H, NH_i), 4.88 (s, 2H, CH_{2j}), 4.47-4.39 (m, 2H, CH_{2k}) and 2.34 (s, 3H, CH_{3l}). Its mass spectrum showed characteristic peaks at m/z 434 (M+) and 436 (M+2).

1-(4-Bromobenzyl)-3-isopropyl-2-imino-2,3-dihydroquinazolin-4(1*H*)-one **(54)** showed IR characteristic peaks at 3301 (N-H str), 1617 (C=O str) and 1534cm^{-1}(C=N str).

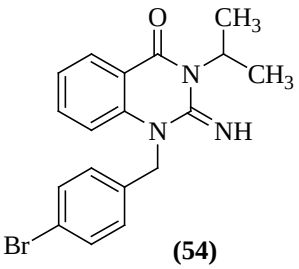

(54)

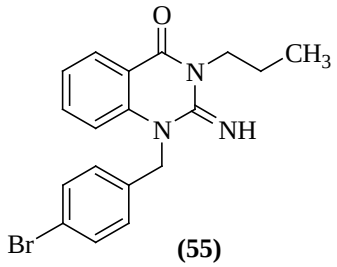

(55)

1-(4-Bromobenzyl)-3-propyl-2-imino-2,3-dihydroquinazolin-4(1*H*)-one **(55)** showed IR characteristic peaks at 3277 (N-H str), 1616 (C=O str) and 1537cm^{-1}(C=N str).

1-(4-Bromobenzyl)-3-cyclopropyl-2-imino-2,3-dihydroquinazolin-4(1*H*)-one **(56)** showed IR characteristic peaks at 3265 (N-H str), 1615 (C=O str) and 1533 cm^{-1}(C=N str). Its ^{1}H-NMR spectrum displayed signals at δ 7.61-7.04 (m, 8H, Ar$H_{a\text{-}f}$), 5.38 (s, 2H, CH_{2g}), 3.20-3.16 (m, 1H, CH_{h}), 1.01-0.96 (m, 2H, CH_{2i}) and 0.73-0.71 (m, 2H, CH_{2j}).

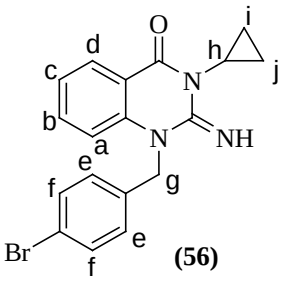

(56)

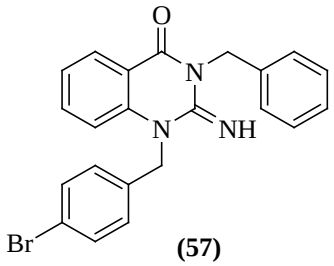

(57)

1-(4-Bromobenzyl)-3-benzyl-2-imino-2,3-dihydroquinazolin-4(1*H*)-one **(57)** showed IR characteristic peaks at 3271 (N-H str), 1615 (C=O str) and 1538cm^{-1}(C=N str).

1-(4-Bromobenzyl)-3-(2-chlorobenzyl)-2-imino-2,3-dihydroquinazolin-4(1*H*)-one **(58)** showed IR characteristic peaks at 3299 (N-H str), 1617 (C=O str) and 1536 cm^{-1}(C=N str). Its ^{1}H-NMR spectrum displayed signals at 7.63-6.93 (m, 12H, Ar$H_{a\text{-}j}$), 6.21 (s, 1H, NH_{k}), 5.39 (s, 2H, CH_{2l}) and 5.03-4.99 (m, 2H, CH_{2m}).

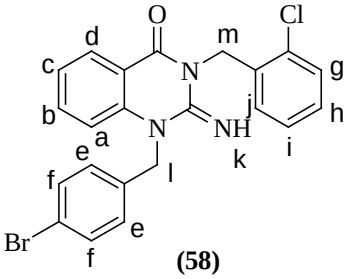

(58)

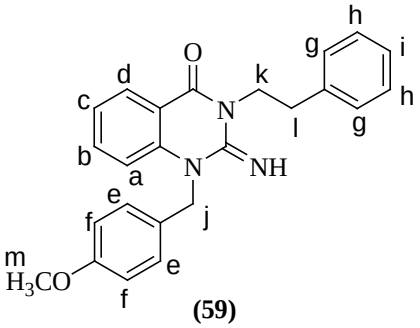

(59)

1-(4-Methoxybenzyl)-3-phenethyl-2-imino-2,3-dihydroquinazolin-4(1*H*)-one **(59)** showed IR characteristic peaks at 3290 (N-H str), 1635 (C=O str) and 1537 cm^{-1}(C=N str). Its ^{1}H-NMR spectrum displayed signals at δ 7.51-6.72 (m, 13H, Ar$H_{a\text{-}i}$), 5.28 (s, 2H, CH_{2j}), 3.93 (t, 2H, CH_{2k}), 3.68 (s, 3H, OCH_{3m}) and 2.97 (t, 2H, CH_{2l}). Its mass spectrum showed M+H peak at m/z 386.1.

3-Isobutyl-1-(4-methoxybenzyl)-2-imino-2,3-dihydroquinazolin-4(1*H*)-one **(60)** showed IR characteristic peaks at 3291 (N-H str), 1616 (C=O str) and 1538 cm^{-1}(C=N str). Its ^{1}H-NMR spectrum displayed signals at δ 7.51-6.72 (m, 8H, Ar$H_{a\text{-}f}$), 5.89 (s, 1H, NH_g), 5.30 (s, 2H, CH_{2h}), 3.68 (s, 3H, OCH_{3l}), 3.49 (d, 2H, CH_{2i}), 2.00-1.93 (m, 1H, CH_j) and 0.95 (d, 6H, CH_{3k}). Its mass spectrum showed M+H peak at m/z 338.4.

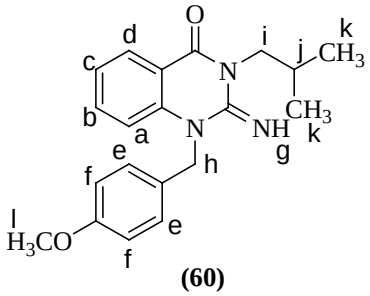

(60)

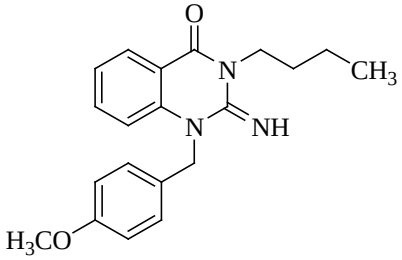

(61)

3-Butyl-1-(4-Methoxybenzyl)-2-imino-2,3-dihydroquinazolin-4(1*H*)-one **(61)** showed IR characteristic peaks at 3274 (N-H str), 1618 (C=O str) and 1542cm^{-1}(C=N str).

1-(4-Methoxybenzyl)-3-(4-methylbenzyl)-2-imino-2,3-dihydroquinazolin-4(1*H*)-one **(62)** showed IR characteristic peaks at 3260 (N-H str), 1617 (C=O str) and 1536 cm^{-1}(C=N str). Its ^{1}H-NMR spectrum displayed signals at δ 7.51-6.81 (m, 12H, Ar$H_{a\text{-}h}$), 5.88 (s, 1H, NH_i), 5.40 (s, 2H, CH_{2j}), 4.86-4.84 (m, 2H, CH_{2k}), 3.76 (s, 3H, OCH_{3l}) and 2.36 (s, 3H, CH_{3m}). Its mass spectrum showed M+H peak at m/z 386.5.

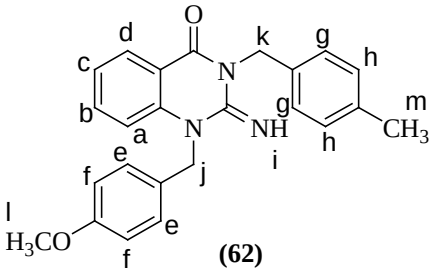

(62)

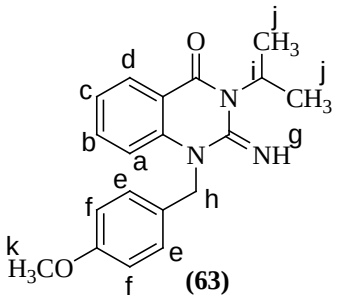

(63)

3-Isopropyl-1-(4-methoxybenzyl)-2-imino-2,3-dihydroquinazolin-4(1*H*)-one **(63)** showed IR characteristic peaks at 3274 (N-H str), 1614 (C=O str) and 1534 cm^{-1}(C=N str). Its ^{1}H-NMR spectrum displayed signals at δ 7.58-6.79 (m, 8H, Ar$H_{a\text{-}f}$), 5.73 (s, 1H, NH_g), 5.37 (s, 2H, CH_{2h}), 4.74-4.72 (m, 1H, CH_i), 3.75 (s, 3H, OCH_{3k}) and 1.33 (d, 6H, CH_{3j}). Its mass spectrum showed M+H peak at m/z 324.1.

3-Benzyl-1-(4-methoxybenzyl)-2-imino-2,3-dihydroquinazolin-4(1*H*)-one **(64)** showed IR characteristic peaks at 3271 (N-H str), 1639 (C=O str) and 1539 cm^{-1}(C=N str). Its ^{1}H-NMR spectrum displayed signals at δ 7.52-6.82 (m, 13H, Ar$H_{a\text{-}i}$), 5.93 (s, 1H, NH_j), 5.40 (s, 2H, CH_{2k}), 4.90 (s, 2H, CH_{2l}) and 3.79 (s, 3H, OCH_{3m}).

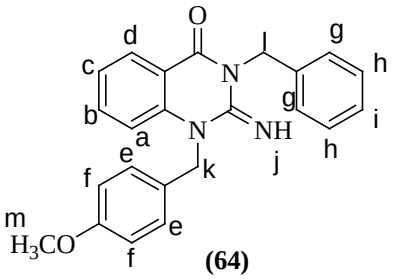

(64)

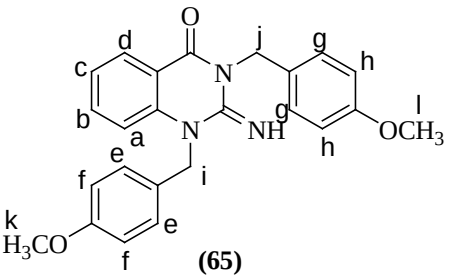

(65)

1,3-bis(4-Methoxybenzyl)-2-imino-2,3-dihydroquinazolin-4(1*H*)-one **(65)** showed IR characteristic peaks at 3253 (N-H str), 1616 (C=O str) and 1535 cm^{-1}(C=N str). Its ^{1}H-NMR spectrum displayed signals at δ 7.65-6.81 (m, 12H, Ar$H_{a\text{-}h}$), 5.37 (s, 2H, CH_{2i}), 4.83 (s, 2H, CH_{2j}), 3.80 (s, 3H, OCH_{3k}) and 3.76 (s, 3H, OCH_{3l}).

3-(2-Chlorobenzyl)-1-(4-methoxybenzyl)-2-imino-2,3-dihydroquinazolin-4(1*H*)-one **(66)** showed IR characteristic peaks at 3276 (N-H str), 1617 (C=O str) and 1537 cm^{-1}(C=N str). Its ^{1}H-NMR spectrum displayed signals at δ 7.58-6.89 (m, 12H, Ar$H_{a\text{-}j}$), 6.29 (s, 1H, NH_k), 5.37 (s, 2H, CH_{2l}), 5.02-4.98 (m, 2H, CH_{2m}) and 3.75 (s, 3H, OCH_{3n}).

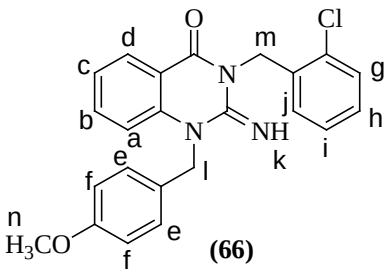

(66)

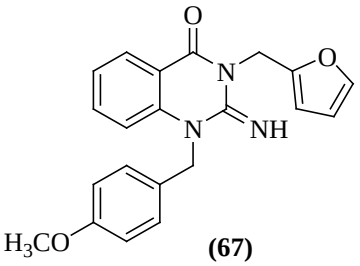

(67)

3-(Furan-2-yl)methyl-1-(4-methoxybenzyl)-2-imino-2,3-dihydroquinazolin-4(1*H*)-one **(67)** showed IR characteristic peaks at 3278 (N-H str), 1617 (C=O str) and 1538 cm^{-1}(C=N str).

1,3-Diphenethyl-2-imino-2,3-dihydroquinazolin-4(1*H*)-one **(68)** showed IR characteristic peaks at 3329 (N-H str), 1615 (C=O str) and 1533 cm^{-1}(C=N str). Its ^{1}H-NMR spectrum displayed signals at δ 7.58 (t, 1H, ArH_g), 7.48 (d, 1H, ArH_a), 7.34-7.20 (m, 11H, Ar$H_{b\text{-}f,h,i}$), 7.09 (t, 1H, ArH_j), 6.10 (bs, 1H, NH_k), 4.39-4.35(m, 2H, CH_{2l}), 3.98-3.93 (m, 2H, CH_{2n}), 3.04-2.99 (m, 4H, C$H_{2m,o}$). Its mass spectrum showed M+H peak at m/z 370.

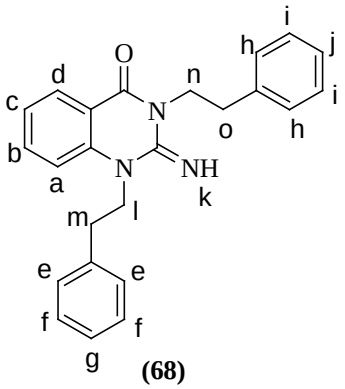

(68)

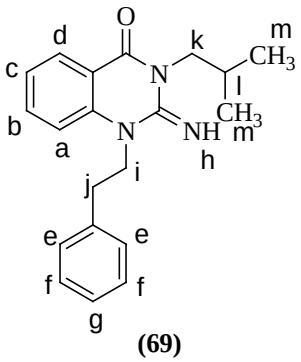

(69)

3-Isobutyl-1-phenethyl-2-imino-2,3-dihydroquinazolin-4(1*H*)-one **(69)** showed IR characteristic peaks at 3274 (N-H str), 1620 (C=O str) and 1540 cm^{-1}(C=N str). Its ^{1}H-NMR spectrum displayed signals at δ 7.67-7.59 (m, 2H, Ar$H_{a,b}$), 7.34-7.15 (m, 7H, Ar$H_{c\text{-}g}$), 6.21 (bs, 1H, NH_h), 4.39-4.35 (m, 2H, CH_{2i}), 3.54 (d, 2H, CH_{2k}), 3.04-3.00 (m, 2H, CH_{2j}), 2.11-2.02 (m, 1H, CH_l) and 1.02 (d, 6H, CH_{3m}). Its mass spectrum showed M+H peak at m/z 322.1.

3-Butyl-1-phenethyl-2-imino-2,3-dihydroquinazolin-4(1*H*)-one **(70)** showed IR characteristic peaks at 3327 (N-H str), 1638 (C=O str) and 1541 cm^{-1}(C=N str). Its ^{1}H-NMR spectrum displayed signals at δ 7.71-7.14 (m, 9H, Ar$H_{a\text{-}g}$), 6.24 (bs, 1H, NH_h), 4.39-4.35 (m, 2H, CH_{2i}), 3.68 (t, 2H, CH_{2k}), 3.02 (t, 2H, CH_{2j}), 1.72-1.65 (m, 2H, CH_{2l}), 1.45-1.40 (m, 2H, CH_{2m}) and 0.94 (t, 3H, CH_{3n}). Its mass spectrum showed M+H peak at m/z 322.4.

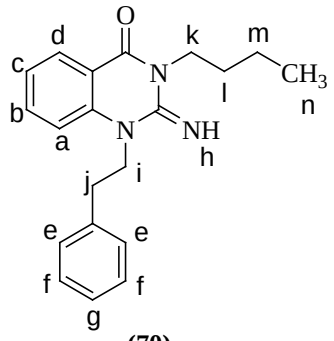

(70)

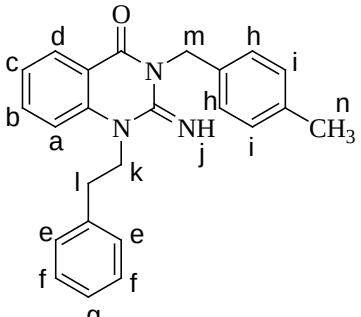

(71)

3-(4-Methylbenzyl)-1-phenylethyl-2-imino-2,3-dihydroquinazolin-4(1*H*)-one **(71)** showed IR characteristic peaks at 3257 (N-H str), 1622 (C=O str) and 1536 cm^{-1}(C=N str). Its ^{1}H-NMR spectrum displayed signals at δ 7.65-7.04 (m, 13H, Ar$H_{a\text{-}i}$), 5.86 (s, 1H, NH_j), 4.82 (s, 2H, CH_{2m}), 4.37 (t, 2H, CH_{2k}), 3.03 (t, 2H, CH_{2l}) and 2.36 (s, 3H, CH_{3n}). Its mass spectrum showed M+H peak at m/z 370.1.

1-Phenethyl-3-propyl-2-imino-2,3-dihydroquinazolin-4(1*H*)-one **(72)** showed IR characteristic peaks at 3274 (N-H str), 1638 (C=O str) and 1542 cm^{-1}(C=N str). Its ^{1}H-NMR spectrum displayed signals at δ 7.72-7.10 (m, 9H, Ar$H_{a\text{-}g}$), 6.48 (s, 1H, NH_h), 4.30 (t, 2H, CH_{2i}), 3.61 (t, 2H, CH_{2k}), 2.95 (t, 2H, CH_{2j}), 1.73-1.65 (m, 2H, CH_{2l}) and 0.94 (t, 3H, CH_{3m}). Its mass spectrum showed M+H peak at m/z 308.4.

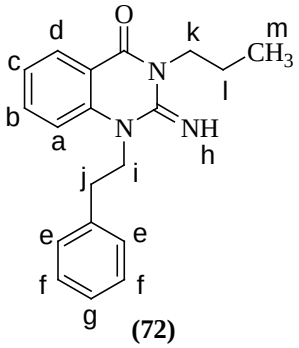

(72)

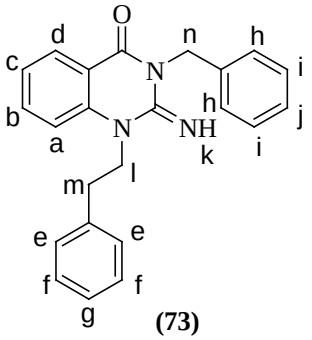

(73)

3-Benzyl-1-phenethyl-2-imino-2,3-dihydroquinazolin-4(1*H*)-one **(73)** showed IR characteristic peaks at 3257 (N-H str), 1622 (C=O str) and 1537 cm^{-1}(C=N str). Its ^{1}H-NMR spectrum displayed signals at δ 7.63-7.11 (m, 14H, Ar$H_{a\text{-}j}$), 5.94 (s, 1H, NH_k), 4.88-4.87 (m, 2H, CH_{2n}), 4.39 (t, 2H, CH_{2l}) and 3.04 (t, 2H, CH_{2m}). Its mass spectrum showed M+H peak at m/z 356.4.

3-(4-Methoxybenzyl)-1-phenethyl-2-imino-2,3-dihydroquinazolin-4(1*H*)-one **(74)** showed IR characteristic peaks at 3255 (N-H str), 1627 (C=O str) and 1538 cm^{-1}(C=N str).

Its ^{1}H-NMR spectrum displayed signals at δ 7.77-6.80 (m, 13H, Ar$H_{a\text{-}i}$), 4.76 (s, 2H, CH_{2j}), 4.3 (t, 2H, CH_{2k}), 3.62 (s, 3H, OCH_{3m}) and 2.96 (t, 2H, CH_{2l}).

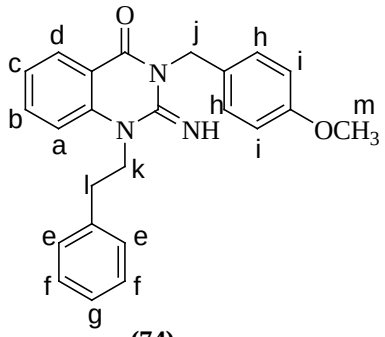

(74)

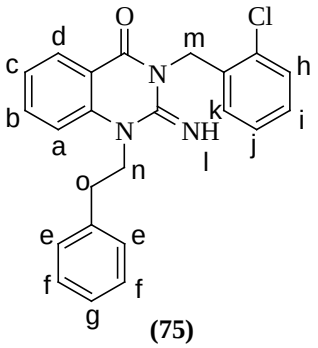

(75)

3-(2-Chlorobenzyl)-1-phenethyl-2-imino-2,3-dihydroquinazolin-4(1*H*)-one **(75)** showed IR characteristic peaks at 3218 (N-H str), 1621 (C=O str) and 1535 cm^{-1}(C=N str). Its ^{1}H-NMR spectrum displayed signals at δ 7.63-7.13 (m, 13H, Ar$H_{a\text{-}k}$), 6.27 (s, 1H, NH_l), 4.98 (s, 2H, CH_{2m}), 4.37 (t, 2H, CH_{2n}) and 3.02 (t, 2H, CH_{2o}). Its mass spectrum showed M+H peak at m/z 390.4.

1-Methyl-3-phenethyl-2-imino-2,3-dihydroquinazolin-4(1*H*)-one **(76)** showed IR characteristic peaks at 3259 (N-H str), 1622 (C=O str) and 1538 cm^{-1}(C=N str). Its mass spectrum showed M+H peak at m/z 280.2.

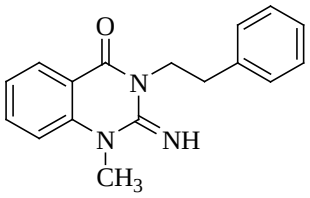

(76)

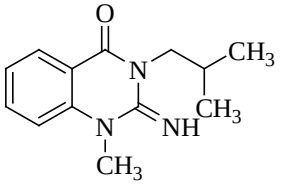

(77)

3-Isobutyl-1-methyl-2-imino-2,3-dihydroquinazolin-4(1*H*)-one **(77**) showed IR characteristic peaks at 3269 (N-H str), 1620 (C=O str) and 1536 cm^{-1}(C=N str).

1-Methyl-3-(4-methylbenzyl)-2-imino-2,3-dihydroquinazolin-4(1*H*)-one **(78)** showed IR characteristic peaks at 3328 (N-H str), 1618 (C=O str) and 1535 cm^{-1}(C=N str). Its ^{1}H-NMR spectrum displayed signals at δ 7.67-7.14 (m, 8H, Ar$H_{a\text{-}f}$), 4.81 (s, 2H, CH_{2g}), 3.62 (s, 3H, CH_{3h}) and 2.33 (s, 3H, CH_{3i}). Its mass spectrum showed M+H peak at m/z 280.3.

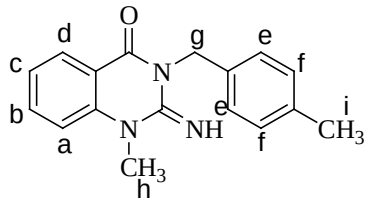

(78)

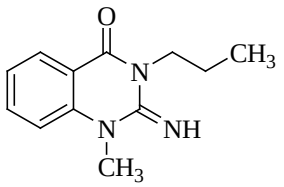

(79)

1-Methyl-3-propyl-2-imino-2,3-dihydroquinazolin-4(1*H*)-one **(79)** showed IR characteristic peaks at 3287 (N-H str), 1620 (C=O str) and 1537 cm^{-1}(C=N str).

3-(2-Chlorobenzyl)-1-methyl-2-imino-2,3-dihydroquinazolin-4(1*H*)-one **(80**) showed IR characteristic peaks at 3259 (N-H str), 1623 (C=O str) and 1539 cm^{-1}(C=N str). Its ^{1}H-NMR spectrum displayed signals at δ 7.65-7.10 (m, 8H, Ar$H_{a\text{-}h}$), 5.77 (s, 1H, NH_{i}), 3.98-3.94 (m, 2H, CH_{2j}) and 3.62 (s, 3H, CH_{3k}).

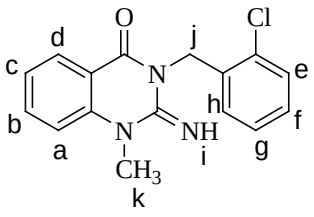

(80)

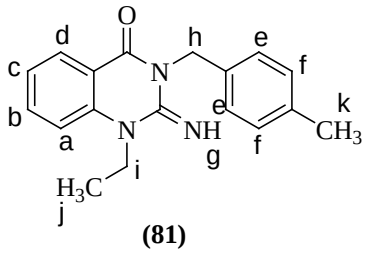

(81)

1-Ethyl-3(4-methylbenzyl)-2-imino-2,3-dihydroquinazolin-4(1*H*)-one **(81)** showed IR characteristic peaks at 3222 (N-H str), 1623 (C=O str) and 1540 cm^{-1}(C=N str). Its ^{1}H-NMR spectrum displayed signals at δ 7.66-7.12 (m, 8H, Ar$H_{a\text{-}f}$), 6.30 (bs, 1H, NH_{g}), 4.80 (s, 2H, CH_{2h}), 4.24 (q, 2H, CH_{2i}), 2.33 (s, 3H, CH_{3k}) and 1.33 (t, 3H, CH_{3j}). Its mass spectrum showed M+H peak at m/z 294.3.

1-Allyl-3-isobutyl-2-imino-2,3-dihydroquinazolin-4(1*H*)-one **(82)** showed IR characteristic peaks at 3294 (N-H str), 1638 (C=O str) and 1537 cm^{-1}(C=N str). Its ^{1}H-NMR spectrum displayed signals at δ 7.55-7.07 (m, 4H, Ar$H_{a\text{-}d}$), 5.91 (br, 1H, NH_{e}), 5.90-5.82 (m, 1H, CH_{g}=CH_2), 5.15-5.10 (m, 2H, CH=CH_{2h}), 4.77-4.75 (m, 2H, CH_{2f}), 3.47 (d, 2H, CH_{2i}), 1.98-1.91 (m, 1H, CH_{j}) and 0.93 (d, 6H, CH_{3k}). Its mass spectrum showed M+H peak at m/z 258.2.

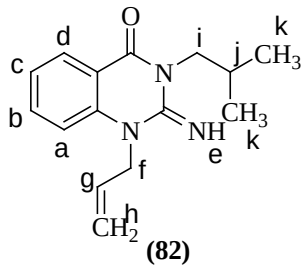

(82)

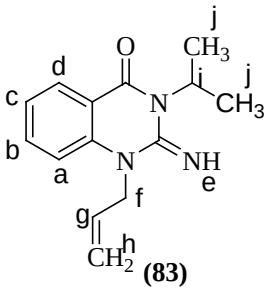

(83)

1-Allyl-3-isopropyl-2-imino-2,3-dihydroquinazolin-4(1*H*)-one **(83)** showed IR characteristic peaks at 3307 (N-H str), 1615 (C=O str) and 1534 cm^{-1}(C=N str). Its ^{1}H-NMR spectrum displayed signals at δ 7.64-7.13 (m, 4H, Ar$H_{a\text{-}d}$), 5.98-5.89 (m, 1H, CH_g=CH_2), 5.82 (bs, 1H, NH_e), 5.21-5.12 (m, 2H, CH=CH_{2h}), 4.83 (d, 2H, CH_{2f}), 4.72-4.67 (m, 1H, CH_i) and 1.30 (d, 6H, CH_{3j}). Its mass spectrum showed M+H peak at m/z 244.3.

1-Allyl-3-cyclopropyl-2-imino-2,3-dihydroquinazolin-4(1*H*)-one **(84)** showed IR characteristic peaks at 3245 (N-H str), 1654 (C=O str) and 1532 cm^{-1}(C=N str).

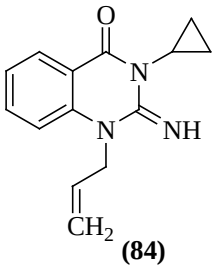

(84)

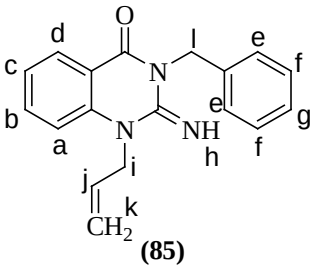

(85)

1-Allyl-3-benzyl-2-imino-2,3-dihydroquinazolin-4(1*H*)-one **(85)** showed IR characteristic peaks at 3224 (N-H str), 1634 (C=O str) and 1535 cm^{-1}(C=N str). Its ^{1}H-NMR spectrum displayed signals at δ 7.62-7.12 (m, 9H, Ar$H_{a\text{-}g}$), 5.99-5.92 (m, 2H, NH_h, CH_j=CH_2), 5.23-5.14 (m, 2H, CH=CH_{2k}) and 4.88-4.85 (m, 4H, CH_{2i} and CH_{2l}).

1-Allyl-3-(2-chlorobenzyl)-2-imino-2,3-dihydroquinazolin-4(1*H*)-one **(86)** showed IR characteristic peaks at 3265 (N-H str), 1632 (C=O str) and 1540 cm^{-1}(C=N str). Its ^{1}H-NMR spectrum displayed signals at δ 7.62-7.13 (m, 8H, Ar$H_{a\text{-}h}$), 6.20 (s, 1H, NH_i), 5.98-5.89 (m, 1H, CH_k=CH_2), 5.22-5.17 (m, 2H, CH=CH_{2l}), 4.99 (d, 2H, CH_{2j}) and 4.84-4.83 (m, 2H, CH_{2m}).

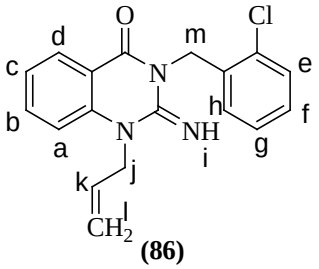

(86)

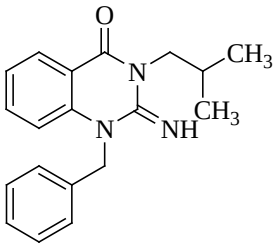

(87)

1-Benzyl-3-isobutyl-2-imino-2,3-dihydroquinazolin-4(1*H*)-one **(87)** showed IR characteristic peaks at 3322 (N-H str), 1637 (C=O str) and 1538 cm^{-1}(C=N str).

1-Benzyl-3-(4-methylbenzyl)-2-imino-2,3-dihydroquinazolin-4(1*H*)-one **(88)** showed IR characteristic peaks at 3267 (N-H str), 1617 (C=O str) and 1535 cm^{-1}(C=N str). Its ^{1}H-NMR spectrum displayed signals at δ 7.51-7.06 (m, 13H, Ar$H_{a\text{-}i}$), 5.94 (s, 1H, NH_j), 5.46 (s, 2H, CH_{2k}), 4.87-4.85 (m, 2H, CH_{2l}) and 2.36 (s, 3H, CH_{3m}). Its mass spectrum showed M+H peak at m/z 356.4.

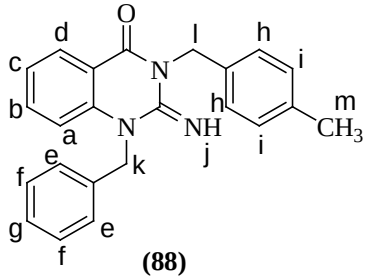

(88)

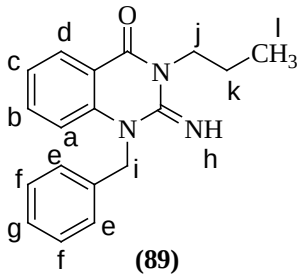

(89)

1-Benzyl-3-propyl-2-imino-2,3-dihydroquinazolin-4(1*H*)-one **(89)** showed IR characteristic peaks at 3276 (N-H str), 1638 (C=O str) and 1540 cm^{-1}(C=N str). Its ^{1}H-NMR spectrum displayed signals at δ 7.76-7.12 (m, 9H, Ar$H_{a\text{-}g}$), 6.56 (s, 1H, NH_h), 5.44 (s, 2H, CH_{2i}), 3.70 (t, 2H, CH_{2j}), 1.81-1.72 (m, 2H, CH_{2k}) and 1.02 (t, 3H, CH_{3l}). Its mass spectrum showed M+H peak at m/z 294.3.

1,3-Dibenzyl-2-imino-2,3-dihydroquinazolin-4(1*H*)-one **(90)** showed IR characteristic peaks at 3270 (N-H str), 1647 (C=O str) and 1540 cm^{-1}(C=N str).

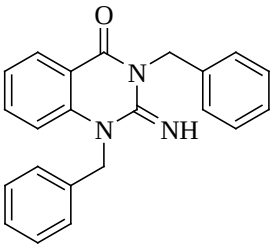

(90)

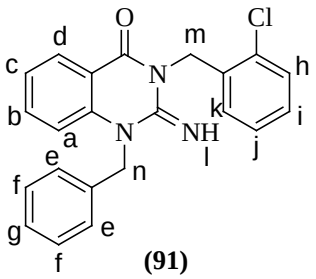

(91)

1-Benzyl-3-(2-chlorobenzyl)-2-imino-2,3-dihydroquinazolin-4(1*H*)-one **(91)** showed IR characteristic peaks at 3304 (N-H str), 1641 (C=O str) and 1540 cm^{-1}(C=N str). Its ^{1}H-NMR spectrum displayed signals at δ 7.61-7.09 (m, 13H, Ar$H_{a\text{-}k}$), 6.21 (bs, 1H, NH_{l}), 5.45 (s, 2H, CH_{2m}), 5.03 (s, 2H, CH_{2n}).

4.2 Biological studies

All the synthesized compounds were screened for their anti-Alzheimer's potential by determining their anticholinesterase activity (Table 4.2). The most promising compound (**75**) was further assessed for its anti-Alzheimer's potential by performing other more sophisticated tests.

4.2.1 The test compounds exhibited good anticholinesterase activity

For preliminary screening of iminoquinazolin-4-one derivatives, *in vitro* anticholinesterase (anti-ChE) activity was assessed using Ellman's assay. Current Alzheimer's treatment includes AChE inhibitors which show their beneficial effects by increased functioning of the existing cholinergic neurons, improved general cognitive functions and reduced behavioural disturbances. However, butyrylcholinesterase (BuChE) is also a key degrading enzyme for ACh during the late phase of the disease where BuChE level remains constant or increases while AChE concentration decreases in certain brain regions.[137-139] Thus, it was logical to check the test compounds for AChE and BuChE inhibitory activities. Among the series, compound (**75**) showed the highest activity by inhibiting AChE and BuChE with IC_{50} values of 5.40±2.96 μM and 7.28±0.27 μM respectively. The results are summarized in Table 4.2.

4.2.2 Compound (75) attenuated A$\beta_{1\text{-}42}$ aggregation

There are evidences indicating that localized AChE and Aβ in senile plaques promoted the assembly of Aβ into fibrils, and accelerated the deposition of Aβ peptide. AChE binds to Aβ directly through its peripheral binding site (PAS) to promote aggregatory effect.[140,141] From the *in vitro* ChE inhibition studies, compound (**75**) from the series with potent AChE inhibitory activity was selected for the thioflavin T (ThT) assay and Congo red (CR) binding assay[142,143] (Table 4.2) to evaluate their ability to inhibit AChE-induced $A\beta_{1-42}$ aggregation. Result showed that the compound (**75**) at 10 μM exhibited significant anti-$A\beta_{1-42}$ aggregatory effects in thioflavin-T (ThT) assay and in CR binding assay (23.67±2.98% and 26.18±2.16% inhibition respectively). The results are summarized in Table 4.2.

Table 4.2: AChE and BuChE inhibitory activities (IC_{50} values) and inhibition of $A\beta_{1-42}$ aggregation by the test compounds

Compound	**Activity[a] IC_{50}**		**% Inhibition of $A\beta_{1-42}$ aggregation[b] (at 10μM)**	
	AChE (μM)	**BuChE (μM)**	**ThT assay**	**CR binding assay**
50	36.23±3.02	11.66±1.20	nd	nd
51	16.89±1.83	2.87±0.19	nd	nd
52	52.03±2.74	23.24±1.61	nd	nd
53	44.76±5.28	55.43±2.71	nd	nd
54	19.74±2.06	10.28±1.52	nd	nd
55	20.88±2.56	560.6±3.84	nd	nd
56	10.55±2.53	101.7±12.9	nd	nd
57	34.88±3.36	82.5±6.45	nd	nd
58	26.37±2.46	106.3±3.73	nd	nd
59	40.99±3.79	24.99±2.15	nd	nd
60	5.92±2.62	8.45±1.12	nd	nd
61	15.53±0.58	14.96±1.22	nd	nd
62	17.34±1.98	3.007±2.06	nd	nd
63	43.08±2.09	5.58±0.61	nd	nd
64	24.66±2.52	8.621±1.74	nd	nd
65	38.27±3.04	53.41±2.25	nd	nd
66	48.53±2.25	2.559±1.14	nd	nd
67	17.31±1.22	25.38±2.28	nd	nd
68	7.72±1.75	150.0±6.21	nd	nd
69	44.45±3.87	86.51±1.82	nd	nd
70	4.73±2.77	15.39±1.39	nd	nd
71	95.21±3.82	6.456±0.77	nd	nd
72	18.69±1.47	35.33±3.77	nd	nd
73	18.42±2.39	77.79±9.88	nd	nd

74	258.9±4.45	106.3±8.50	nd	nd
75	**5.40±2.96**	**7.28±0.27**	**23.67±2.98**	**26.18±2.16**
76	15.18±0.32	8.73±0.38	nd	nd
77	6.237±0.17	19.48±1.98	nd	nd
78	2.44±2.55	27.12±1.63	nd	nd
79	10.87±1.28	20.48±2.56	nd	nd
80	47.45±1.90	18.37±1.09	nd	nd
81	15.73±1.12	40.88±1.61	nd	nd
82	16.83±3.01	32.13±1.15	nd	nd
83	6.88±2.14	24.16±1.22	nd	nd
84	6.967±0.70	6.542±0.35	nd	nd
85	69.85±3.89	9.017±1.30	nd	nd
86	22.07±2.68	18.86±2.61	nd	nd
87	7.141±2.60	7.554±0.70	nd	nd
88	21.93±2.35	1.876±1.48	nd	nd
89	15.77±1.88	7.78±0.23	nd	nd
90	7.366±2.63	2.274±0.31	nd	nd
91	18.23±1.82	8.262±1.71	nd	nd
Tacrine	12.72±2.36(nM)	2.13±0.10 (nM)	10.63±1.28	nd
Donepezile	4.55±1.38(nM)	1.108±1.11	37.26±2.69	nd

[a] AChE and BuChE inhibitory activities (IC_{50} values) and [b] Inhibition of $A\beta_{1-42}$ aggregation produced by the test compounds at 10 μM. Results are the mean ± SEM of at least three determinations. nd=Not determined.

4.2.3 Test compound (75) showed neuroprotective effect in SH-SY5Y cells

To check therapeutic suitability of the selected test compound, its effect on cell viability and neuroprotective activity against oxidative stress were evaluated using the human neuroblastoma SH-SY5Y cell line. For assessment of cytotoxicity of the test compound, cells were exposed to relatively high concentrations of the test compound (40 μM and 80 μM) for 24 hr followed by determination of the cell viability using 3-(4,5-dimethylthiazol-2-yl)-2,5-diphenyltetrazolium bromide (MTT) assay. Results showed negligible cell death even at such a high concentrations (Table 4.3). In another set of experiments, neuroprotective potential of the selected test derivative was assessed. Oxidative stress-like condition in SH-SY5Y cells was induced using H_2O_2 as a toxic insult.[144,145] In this assay, addition of H_2O_2 (100 μM) to the growth medium caused significant cell death as evidenced by reduction in cell viability (52-56 %) compared to the control. To assess the neuroprotective potential of the test compound against the toxic attack of H_2O_2, the cells were pre-treated for 2 hr with the test compound (5 μM, 10 μM

and 20 μM) followed by H_2O_2 treatment for 24 hr. The compound (**75**) showed insignificant neuroprotective effect at 10 μM and 20 μM concentrations. (Table 4.3)

Table 4.3: Cell viability, neuroprotection and free radical scavenging activity of the test compound (**75**) in the human neuroblastoma SH-SY5Y cell line and DPPH assay

Compound	**Cell Viability (%)**		**Neuroprotection (%)**		**RP of DPPH (%)**	
	40 μM	**80 μM**	**10 μM**	**20 μM**	**10 μM**	**20 μM**
75	94.4±2.5	92.6±2.8	27.2±2.5	43.8±3.9	44.4±3.5	60.2±3.4
Tacrine	89.4±2.3	90.0±3.4	44.7±3.3	57.9±2.1	54.9±2.1	68.8±3.7
Donepezil	96.9±1.4	92.3±2.4	48.2±2.4	62.0±2.5	59.9±2.6	75.5±2.9
Ascorbic acid	nd	nd	nd	nd	56.4±2.7	67.7±2.7

Percentage cell viability of SH-SY5Y cells exposed to relatively high concentrations (40 μM and 80 μM) of test compound. Percentage neuroprotection of SH-SY5Y cells at relatively lower concentrations (10 μM and 20μM) of the test compound against H_2O_2 (100 μM) insult. RP of DPPH **(%) =** reduction percentage of DPPH. Results are the mean ± SEM of at least three independent experiments. nd = not determined.

4.2.4 Test compound (75) showed antioxidant activity in DPPH assay

2,2-Diphenyl-1-picrylhydrazyl (DPPH) is one of the few stable and commercially available organic nitrogen radicals. DPPH assay is commonly used for preliminary screening of compounds capable of scavenging activated oxygen species.[146] The compound (**75**) was evaluated for its antioxidant potential using DPPH assay which shows significant 44 % and 60 % free radical scavenging activity at 10 μM and 20 μM concentrations respectively.

4.2.5 Test compound (75) showed enhanced spatial learning ability in MWM test

Compound (**75**) with already proven *in vitro* ChE inhibition activity was further evaluated using the *in vivo* scopolamine-induced amnesic mice model. Scopolamine-induced amnesia in rodents is an accepted standard model in behavioural pharmacology for evaluation of ChE inhibiting anti-Alzheimer's drug candidates. Scopolamine distinctly blocks muscarinic cholinergic receptors that lead to impairment of cognitive functions. MWM test was adopted for the assessment of spatial learning and memory. As shown in Fig. 4.1-A, the scopolamine-treated control animals (1.4 mg/kg, i.p.) showed significant rise in ELT as compared to the vehicle-treated control animals in all trial sessions (p<0.001) indicating scopolamine-induced memory impairment. However, treatment with

75 (10 mg/kg, p.o.) (Fig. 4.1-A, $p<0.001$) significantly reduced the ELT, from third day onward in the probe trial session as compared to the scopolamine-treated control group. Additionally, spatial learning ability was evaluated by counting the number of crossings over the platform area. Standard drug donepezil (at 5 mg/kg, p.o.) significantly reduced ELT (Fig. 4.1-A, $p<0.001$ and Fig. 4.1-A, $p<0.001$) and increased platform area crossings (Fig. 4.1-B, $p<0.01$ and Fig. 4.1-B, $p<0.01$) as compared to the scopolamine-treated control group. Scopolamine-treated control group animals had shown reduced number of platform crossings during all the trial sessions as compared to the vehicle-treated control animals (Fig. 4.1-B, $p<0.01$ and 4.1-B, $p<0.001$) which was significantly increased by **75** (10 mg/kg, p.o.) (Fig. 4.1-B, $p<0.01$) showing its potential to improve spatial learning and memory, which were impaired by scopolamine.

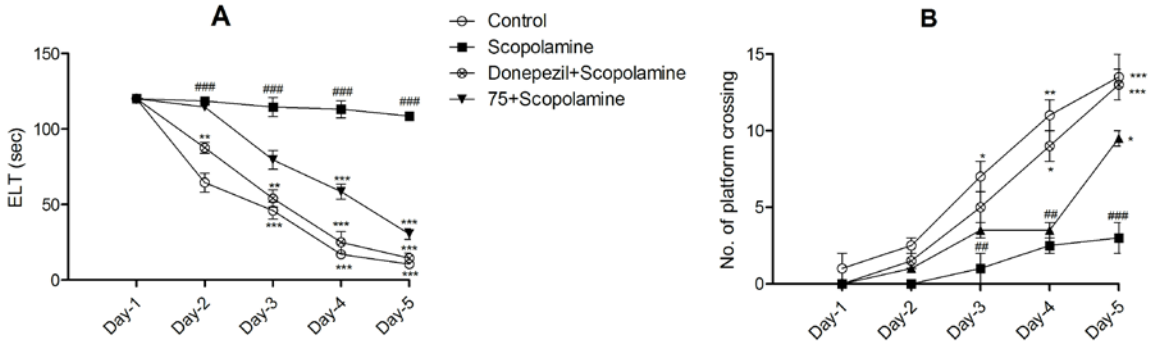

Fig. 4.1: Test compound (**75**) enhanced spatial learning ability of scopolamine-induced amnesic mice in MWM test. Scopolamine treatment (1.4 mg/kg, i.p.) increased the ELT during probe trial sessions, and reduced the number of platform area crossings as compared to the vehicle-treated control mice (A and B). **75** (10 mg/kg, p.o.) (A & B) significantly reversed these alterations similar to donepezil (5 mg/kg, p.o.). Data are expressed as mean ± SEM (n=6). $^{###}p<0.001$, $^{##}p<0.01$ vs. Vehicletreated control group. *** $p<0.001$, ** $p<0.01$, * $p<0.05$ vs. scopolamine-treated control group.

4.2.6 Test compound (75) improved "spontaneous alteration" behaviour in Y maze test

Protection against the damage caused by ICV injection of $A\beta_{1-42}$ in the hippocampal region of rat brain is a promising model to evaluate the neuroprotective potential of a drug candidate in AD-like condition.[147,148] Y maze test was performed to determine the effect of compound (**75**) on "spontaneous alteration" behaviour which is an indicator of immediate working memory. The percentage of "spontaneous alterations" in

the $A\beta_{1-42}$-treated control rats got significantly reduced throughout the training session which was significantly increased by pre-treatment of the animals with **75** (10 mg/kg, p.o.) (Fig. 4.2-A, $p<0.01$) suggesting ability to improve hippocampal dependant immediate working memory.

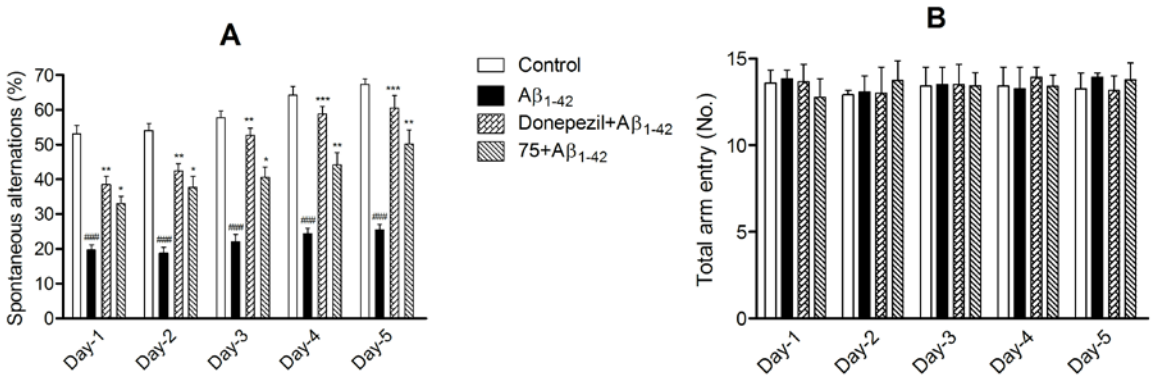

Fig. 4.2: Test compound (**75**) restored immediate working memory impairment induced by ICV injection of Aβ1-42 in hippocampal region of rat brains as observed in Y maze test. The Y maze test was performed during the last five days of treatment period. Donepezil (5 mg/kg, p.o.) and **75** (10 mg/kg, p.o.) was administered to the rats 1 hr prior to the Y-maze task of 5 min duration. (Fig A) $A\beta_{1-42}$ treatment reduced "spontaneous alteration" behaviour which was significantly improved by **75** (Fig B). Mean number of the arm entries remained similar across all animal groups suggesting that locomotor activity was not altered with $A\beta_{1-42}$. Data are expressed as mean ± SEM (n=6). $^{###}p<0.001$ *vs.* vehicle-treated control group. $^{***}p<0.001$, $^{**}p<0.01$, $^{*}p<0.05$ *vs.* $A\beta_{1-42}$-treated control group.

4.2.7 Test compound (75) possessed ROS scavenging activity

ROS scavenging activity was performed to evaluate antioxidant profile of the test compound. Elevated level of ROS is a sign of increased oxidative stress in a variety of pathological conditions.[149] $A\beta_{1-42}$ insult is known to induce oxidative stress in AD pathogenesis.[150] Hence, antioxidant potential of the test compound (**75**) was further confirmed using DCFH-DA assay. $A\beta_{1-42}$-treated (10 μM) rat hippocampal neurons significantly increased ROS generation (Fig. 4.3-A, $p<0.001$) which was significantly reduced with pre-treatment of **75** (10-40 μM) (Fig. 4.3-A, $p<0.001$) showing its ability to reduce toxicity of hippocampal neurons through $A\beta_{1-42}$-treatment. In another set of experiments (Fig 4.3-B), the test compounds (**75**) attenuated apoptosis rate in primary rat hippocampal neurons as assessed by flow cytometry using Annexin V-FITC and PI staining. Cells in the lower left quadrant are viable (Annexine V-FITC-/PI-). Cells in the

lower right quadrant are early apoptotic (Annexine V-FITC+/PI-) and those in the upper right quadrant are late apoptotic or nacrotic (Annexine V-FITC+/PI+).

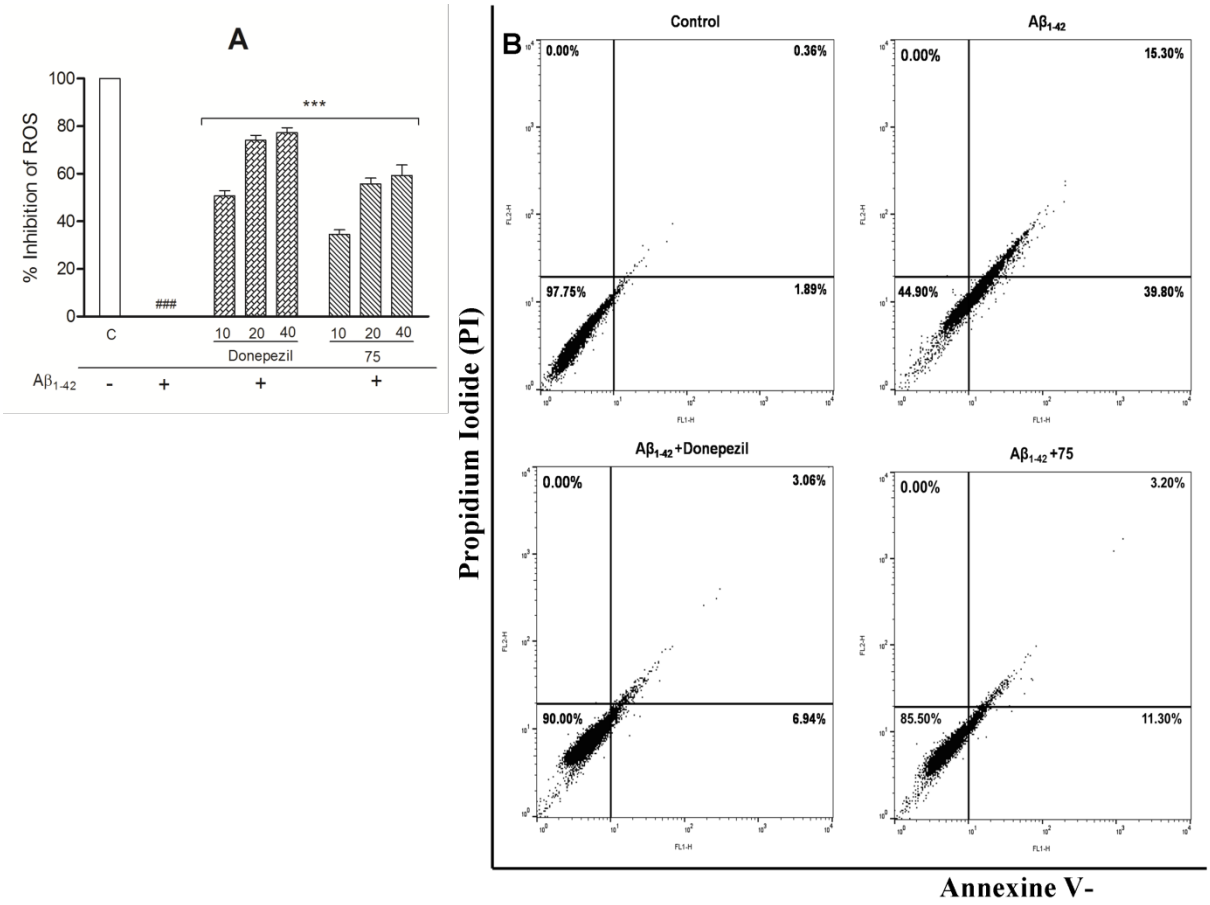

Fig. 4.3: *In vitro* ROS scavenging and antiapoptotic effects of test compound (**75)** against $A\beta_{1-42}$-induced toxicity of hippocampal neurons. $A\beta_{1-42}$ (10 μM) significantly increased ROS generation as compared to the control cells which was significantly reduced by **75** (10-40 μM) (Fig A). Treatment with $A\beta_{1-42}$ (10 μM) significantly increased percentage of early apoptotic cells which was attenuated by pre-treatment with **75** (Fig B) similar to donepezil. Data are expressed as mean ± SEM. $^{###}p<0.001$ *vs.* control cells. *** $p<0.001$, ** $p<0.01$ *vs.* $A\beta_{1-42}$-treated control cells. C=control cells.

In conclusion, the present study has revealed anticholinesterase potential of the novel iminoquinazoline-4-one derivatives through acetylcholinesterase and butyrylcholinesterase inhibitory activity. The most active compound (**75**) in the series was further tested for other aspects to control neuronal loss in the AD. Compound **(75)** has shown the ability to interact with different AD targets as it has shown significant multiple effects including anti-ChE, anti-Aβ aggregatory, neuroprotective, ROS scavenging and antioxidant activities in different *in vitro* and *in vivo* experimental models.